advantage over rest-redistribution ^{201}Tl imaging, which requires 4–24 hr for delayed imaging.

CONCLUSION

Image quality as well as the presence, location and severity of defects are similar under fasting and nonfasting conditions with ^{123}I-IPPA. Therefore, fasting is not necessary before ^{123}I-IPPA SPECT imaging for the assessment of myocardial viability.

ACKNOWLEDGMENTS

This research was supported in part by a research grant from Medco Research, Inc., (Research Triangle Park, NC). We thank Michael McMahon, CNMT, for technological support, as well as Elizabeth Doucette for manuscript preparation. Presented in part at the Annual Meeting Scientific Sessions, Society of Nuclear Medicine, Denver, Colorado, June, 1996.

REFERENCES

1. Braunwald E, Pasternak RC, Sobel BE. Chronic ischemic heart disease. In: Braunwald E, ed. *Heart disease: a textbook of cardiovascular medicine*. Philadelphia: WB Saunders Co.; 1992:1293–1352.
2. Rahimtoola SH. Coronary bypass surgery for chronic angina-1981: a perspective. *Circulation* 1982;65:225–241.
3. Braunwald E, Kroner RA. The stunned myocardium: prolonged, postischemic ventricular dysfunction. *Circulation* 1982;66:1146–1149.
4. Braunwald E, Rutherford JD. Reversible ischemic left ventricular dysfunction: evidence for "hibernating" myocardium. *J Am Coll Cardiol* 1986;8:1467–1470.
5. Rahimtoola SH. The hibernating myocardium. *Am Heart J* 1989;117:211–213.
6. Bolli R. Mechanism of myocardial stunning. *Circulation* 1990;82:723–738.
7. Lewis SJ, Sawada SG, Ryan T, Segar DS, Armstrong WF, Feigenbaum H. Segmental wall motion abnormalities in the absence of clinically documented myocardial infarction: clinical significance and evidence of hibernating myocardium. *Am Heart J* 1991;121:1088–1094.
8. Dilsizian V, Bonow RO. Current diagnostic techniques of assessing myocardial viability in patients with hibernating and stunned myocardium. *Circulation* 1993;87: 1–20.
9. Rankin JS, Newman GE, Muhlbaier LH, et al. The effects of coronary revascularization of left ventricular function in ischemic heart disease. *Thorc Cardiovasc Surg* 1985;90:818–826.
10. Chatterjee K, Swan HJC, Parmley WW, Sustaita H, Marcus HS, Matlott J. Influence of direct myocardial revascularization on left asynergy and function in patients with coronary heart disease: with and without previous myocardial infarction. *Circulation* 1973;47:276–286.
11. Udelson JE, Coleman PS, Metherall J, et al. Predicting recovery of severe regional ventricular dysfunction: comparison of resting scintigraphy with ^{201}Tl and ^{99m}Tc-sestamibi. *Circulation* 1994;89:2552–2561.
12. Kauffman GJ, Boyne TS, Watson DD, Smith WH, Beller GA. Comparison of rest thallium-201 imaging and rest technetium-99m sestamibi imaging for assessment of myocardial viability in patients with coronary artery disease and severe left ventricular dysfunction. *J Am Coll Cardiol* 1996;27:1592–1597.
13. Chien KR, Han A, White J, et al. In vivo esterification of synthetic ^{125}I fatty acid into cardiac glycerolipids. *Am J Physiol* 1983;245:693–697.
14. Reske SN, Schon S, Eichelkraut W, et al. Flow dependence of uptake of (^{123}I-phenyl) pentadecanoic acid in the canine heart. *J Nucl Med* 1983;24:12–15.
15. Sloof GW, Visser FC, Van Eenige MJ, et al. Comparison of uptake, oxidation, and lipid distribution of 12-iodoheptadecanoic acid, 15-(p-iodophenyl) pentadecanoic acid, and 15-(p-iodophenyl)-3,3-dimethylpentadecanoic acid in normal canine myocardium. *J Nucl Med* 1993;34:649–657.
16. Pippin JJ, Jansen DE, Henderson EB, et al. Myocardial fatty acid utilization at various workloads in normal volunteers: iodine-123 phenylpentadecanoic acid and single photon emission computed tomography to investigate myocardial metabolism. *Am J Card Imaging* 1992;6:99–108.
17. Ugolini V, Hansen CL, Kulkarni PV, et al. Abnormal myocardial fatty acid metabolism in dilated cardiomyopathy detected by ^{123}I phenylpentadecanoic acid and tomographic imaging. *Am J Cardiol* 1988;62:923–928.
18. Wolfe CL, Kennedy PL, Kulkarni P, et al. Iodine-123 phenylpentadecanoic acid myocardial scintigraphy in patients with left ventricular hypertrophy: alterations in ventricular distribution and utilization. *Am Heart J* 1990;119:1338–1347.
19. Vyska K, Stremmel W, Notohamiprodjo G, et al. Fatty acid uptake in normal human myocardium. *Circ Res* 1991;69:857–870.
20. Kennedy PL, Corbett JR, Kulkarni PV, et al. Iodine-123-phenylpentadecanoic acid myocardial scintigraphy: usefulness in the identification of myocardial ischemia. *Circulation* 1986;74:1007–1015.
21. Hansen CL, Corbett JR, Pippin J, et al. Iodine-123 phenylpentadecanoic acid and single photon emission computed tomography in identifying left ventricular regional metabolic abnormalities in patients with coronary heart disease: comparison with thallium scintigraphy. *J Am Coll Cardiol* 1988;12:78–87.
22. Murray G, Schad N, Ladd W, et al. Metabolic cardiac imaging in severe coronary artery disease: assessment of viability with iodine-123-iodophenylpentadecanoic acid and multicrystal gamma camera and correlation with biopsy. *J Nucl Med* 1992;33: 1269–1277.
23. Murray G, Schad N, Magill L, Vander Zwaag R. Myocardial viability assessment with dynamic low-dose iodine-123-iodophenylpentadecanoic acid metabolic imaging: comparison with myocardial biopsy and reinjection SPECT thallium after myocardial infarction. *J Nucl Med* 1994;35:43S–48S.
24. Iskandrian AS, Powers J, Cave V, et al. Assessment of myocardial viability by dynamic tomographic iodine-123 iopophenylpentadecanoic acid imaging: comparison with rest-redistribution thallium-201 imaging. *J Nucl Card* 1995;2:101–109.
25. Hansen CL, Heo J, Oliner C, et al. Prediction of improvement in left ventricular function with ^{123}I-IPPA after coronary revascularization. *J Nucl Med* 1995;36:1987–1993.
26. Cohen J. A coefficient of agreement for nominal scales. *Educ Psychol Measure* 1960;20:37–46.
27. McNemar Q. Note on the sampling error of the difference between correlated preparations or percentages. *Psychometrika* 1947;12:153–157.

High-Resolution Cardiac PET in Rabbits: Imaging and Quantitation of Myocardial Blood Flow

Kazuhiro Shimada, Katsuya Yoshida, Hiroyuki Tadokoro, Shinobu Kitsukawa, Akira Takami, Kazutoshi Suzuki, Shuji Tanada and Yoshiaki Masuda

Division of Advanced Technology for Medical Imaging, National Institute of Radiological Sciences, and Third Department of Internal Medicine, Chiba University School of Medicine, Chiba, Japan

A high-resolution PET system for small animals was tested for its applicability to the investigation of regional myocardial blood flow (MBF) in rabbits. **Methods:** Nineteen measurements were performed in 10 closed-chest anesthetized rabbits at baseline and during infusions of adenosine (0.2 mg/kg/min) and propranolol (0.20–1.20 mg slow infusion) to obtain a wide range of MBF. Myocardial blood flow was assessed both by dynamic ^{13}N-ammonia PET and by colored microspheres. Blood was withdrawn directly from the femoral artery, and arterial ^{13}N activity was measured by coincidence type gamma detection system for the input function. Nitrogen-13 myocardial uptake was calculated by dividing the myocardial ^{13}N activity by the integral value of the input function. **Results:** Three or four contiguous cross-sectional myocardial images were obtained after ^{13}N-ammonia injection. The left ventricular wall and cardiac cavity were clearly visualized. Moreover, initial passage of the tracer through the heart was obtained with serial 10-sec PET images. Nitrogen-13 myocardial uptake correlated well with flow measured with microspheres ($r = 0.88$). **Conclusion:** Our cardiac PET system can be used for in vivo imaging and quantitation of MBF in small animals and may play an important role in the future study of animal models of cardiovascular diseases.

Key Words: PET; rabbits; myocardial blood flow

J Nucl Med 1998; 39:2022–2027

Received Dec. 30, 1997; revision accepted Apr. 13, 1998.

For correspondence or reprints contact: Katsuya Yoshida, MD, Division of Advanced Technology for Medical Imaging, National Institute of Radiological Sciences, Anagawa 4-9-1, Inage-ku, Chiba-shi, 263, Japan.

Before new radiopharmaceuticals are clinically applied for nuclear medicine, small animal experiments must be performed to determine the kinetics of the tracer. Small animal PET is expected to make this process precise and efficient (*1*). It is also useful to compare PET images with tissue pathology or invasive measurements of physiologic variables, such as regional blood flow. Although there are several reports concerning PET imaging using small animals (*2–6*), no systems for quantitative cardiac studies have been reported to date. The purpose of this study was to develop a cardiac PET system for small animals. We chose rabbits because they have been frequently used for studies of chronic cardiovascular diseases, such as atherosclerosis (*7*). To assess the quantitation of this system, we chose ^{13}N-ammonia as the tracer and compared its uptake with blood flow measured with microspheres. Tomography was performed using a small animal PET device (SHR-2000; Hamamatsu Photonics K.K., Hamamatsu, Japan). Table 1 presents the physical description and imaging characteristics of this instrument (*8,9*).

MATERIALS AND METHODS

Animal Preparation

Ten male Japanese white rabbits, weighing 2.1–3.9 kg, were studied. Animals were anesthetized with pentobarbital (35 mg/kg) intravenously via the right marginal ear vein. Anesthesia was maintained by a constant intravenous infusion of pentobarbital at 6 mg/kg/hr, beginning 1 hr after induction. Surgical sites were surface-anesthetized with 1% lidocaine. The rabbits were ventilated by tracheotomy using a small animal ventilator (SN-480–5; Shinano, Tokyo, Japan). The settings of this ventilator and the oxygen content of inspired air were adjusted to maintain the blood gases in a physiologic range throughout the experimental period. Blood gases were analyzed using a Ciba–Corning pH/Blood Gas Analyzer (model no. 238; Chiron Diagnostics, Emeryville, CA). The rabbits were paralyzed with pancuronium bromide (0.3 mg/kg intravenously), followed by 0.15 mg/kg intravenously every 40–50 min. Rectal body temperature was maintained at 38–39°C with a heating pad. The right femoral artery was cannulated for collection of the microsphere reference sample and for arterial input function; the left femoral artery was cannulated for the measurement of blood pressure (BP); the right jugular vein was cannulated for the infusion of adenosine, propranolol and normal saline; and the left marginal ear vein was cannulated for the injection of ^{13}N-ammonia. The right carotid artery was cannulated for the injection of 15-μm colored polystyrene microspheres (E-Z Trac, Los Angeles, CA) via a polyethylene catheter (0.87 mm inner diameter, 1.27 mm outer diameter; Natume, Tokyo, Japan) advanced into the left ventricle. The animals were heparinized (400 units/kg) after the cannulations. Arterial pressures and heart rates were monitored with a multichannel polygraph (Omniace RT3200N; NEC San-ei, Tokyo, Japan). The rabbits were then placed in a supine position within the animal PET device. All procedures were approved by the Animal Welfare Committee of the National Institute of Radiological Sciences.

PET

PET images were obtained using a small animal PET (SHR-2000) that provided seven transaxial slices simultaneously. The slices had a transaxial resolution of 3.0 mm FWHM and were separated by 6.5 mm. Axial resolution was 4.8 and 4.1 mm FWHM in direct and cross-planes, respectively (Table 1).

Initially, blank and transmission scans were acquired using a ^{68}Ge/^{68}Ga source for the correction of detection efficiency and photon attenuation. Subsequently, 111 MBq of ^{13}N-ammonia were injected intravenously from the marginal ear vein as a 20-sec slow bolus. Simultaneously, an initial set of six 10-sec data were acquired, followed by six 20-sec and three 1-min data. Blank and transmission data contained 70–80 million and 5–8 million counts in total slices, respectively. Emission data contained 0–0.5 million counts in the early 10-sec scans and 0.9–1.2 million counts in the late 1-min scans in total slices.

The reconstructed images were obtained using a parallel processing system (NuSprint; YARC Systems Corp., Newbury Park, CA) on a personal computer (Macintosh Quadra950; Cupertino, CA) and transferred to a graphics workstation (Indigo2; Silicon Graphics, Mountain View, CA) for further processing. Each image was displayed as 180 × 180 pixels, with a pixel size of 1.0 mm × 1.0 mm. Count losses at the high counting rates were corrected. All reconstructions were corrected for physical decay of the tracer.

Experimental Protocols

The rabbits were allowed to stabilize for 20–30 min after completion of the procedures. Approximately 1.0×10^6 colored microspheres were dispersed with a mechanical mixer immediately before injection and injected into the left ventricle. Blood withdrawal began 15 sec before microsphere injection at a constant rate of 1.5 ml/min to collect microspheres and obtain arterial input function with BACC-4 (Hamamatsu Photonics K.K.). Immediately after the injection of microspheres, ^{13}N-ammonia was administered as a 20-sec slow bolus while the imaging sequence started. PET images were then acquired. Blood withdrawal was stopped 2 min

TABLE 1
Physical Description and Performance Characteristics of High-Resolution PET Device (Hamamatsu SHR-2000) for Small Animals

Detector (crystal material)	Bismuth germanate
Bismuth germanate crystal size	1.7 mm (width) × 10 mm (height) × 17 mm (depth)
No. of detectors	495/ring
No. of rings	4
Ring diameter	348 mm
Ring separation	13 mm
Opening diameter	220 mm
Field of view	
Transaxial	170 mm
Axial	47 mm
Scanning motion	Small angle rotation (24°)
Spatial resolution (center)	
Transaxial	3.0 mm FWHM
Axial	4.8 mm FWHM (direct plane)
	4.1 mm FWHM (cross-plane)
Sensitivity	559 kcps/MBq/ml
(10-cm-diameter cylindrical phantom, 300 keV)	

TABLE 2
Summary of Hemodynamic Data and Myocardial Blood Flow During Various Pharmacologic Interventions

Intervention	Heart rate (beats/min)	Systolic BP (mmHg)	RPP* (mmHg · beat/min)	MBF (ml/min/g)
Control (n = 7)	316 ± 34	120 ± 14	38,007 ± 6,766	3.29 ± 1.04
Adenosine (n = 5)	293 ± 57	95 ± 14†	27,923 ± 7,564	6.16 ± 1.63†,‡
Propranolol (n = 7)	244 ± 31†	117 ± 14	28,590 ± 5,304†	1.63 ± 0.76†

*RPP was calculated as the product of systolic blood pressure (BP) and heart rate.
†$p < 0.05$ vs. control.
‡$p < 0.05$ vs. propranolol.

after the tracer injection. Low molecular weight dextran was infused into the ear vein at a rate of 1.5 ml/min, concurrent with the withdrawal of the blood sample, to prevent a significant decrease in BP during withdrawal. Intravenous infusions of adenosine and propranolol were performed to achieve a wide range of myocardial blood flow (MBF). Two rabbits were studied without any pharmacologic intervention. In five rabbits, myocardial hyperemia was induced with intravenous adenosine. MBF was measured under the preadenosine control condition and during the continuous infusion of adenosine. Adenosine at a concentration of 0.2 mg/kg/min was infused for 9 min. At 3 min after the start of adenosine infusion, microspheres and ^{13}N-ammonia were administered. To evaluate low flow, several doses of propranolol (0.20–1.20 mg slow infusion) were injected in three rabbits. These rabbits received two or three sets of microspheres and ^{13}N-ammonia after propranolol infusion in different hemodynamic states. Therefore, MBF was evaluated during 19 flow states in 10 rabbits. At the end of the studies, the animals were killed during deep anesthesia with KCl solution, the hearts were removed and the left ventricular myocardium was dissected. The whole left ventricular myocardium was weighed, counted in a well counter (Minaxi γ; Packard Instrument, Downers Grove, IL) and corrected for radioactive decay.

The extraction of microspheres from the blood and tissue samples was performed as described by Hale et al. (*10*). Regional MBF was calculated from the formula: regional MBF = $C_m \times Q_r/C_r$, where C_m represents the total number of microspheres/g of myocardial tissue, Q_r is the withdrawal rate of the reference blood sample (ml/min) and C_r is the total number of microspheres in the reference blood sample.

Data Analysis

Nitrogen-13 Myocardial Uptake. Nitrogen-13 myocardial uptake (extraction times flow) was calculated using the following equation (*11*):

$$E \times F = \frac{C_m(t)}{\int_0^t C_a(x)dx \times g},$$

where E is the extraction fraction of ^{13}N-ammonia, F is the MBF (ml/min/g), $C_m(t)$ and $C_a(t)$ are the ^{13}N activity concentrations in the myocardium and arterial blood concentrations at time t, and g is the specific gravity of the myocardium (1.05 g/ml). In this study, ^{13}N myocardial uptake was calculated during the first 3 min of data acquisition (t = 3 min).

Myocardial Nitrogen-13 Activity. Myocardial ^{13}N activity was determined by the following procedure. A region of interest (ROI) on the left ventricular myocardium was drawn at a level of 50% of peak activity for the midventricular slice of a late PET image (3–6 min) and projected to early dynamic images. The ROI size was ~190 pixels. A calibration factor was determined from the ratio of cpm/g of tissue in the well counter to the cpm per ROI recorded with PET (a late PET image, 3–6 min). Subsequently, myocardial ^{13}N activity was expressed in cpm/g.

Arterial Input Function

The high-detection efficiency bismuth germanate (BGO) coincidence detection system (BACC-4) was designed and built for applications involving arterial blood sampling in small animals and PET. The detection system uses four BGO detectors in a configuration to provide a small central opening with very high sensitivity for insertion of small-volume flow-through blood-sampling tubing. Blood was withdrawn from the right femoral artery through the tubing at constant flow (1.5 ml/min) with a Harvard pump (model no. 11; Harvard Apparatus, Millis, MA), which allowed the simultaneous collection of colored microspheres. Further details of this system have been reported elsewhere (*12*). To calibrate this system to the well counter, we obtained serial blood samples from the ascending aortic catheter immediately after ^{13}N-ammonia intravenous injection of five rabbits. In each rabbit, blood sampling was performed under control and adenosine (0.2 mg/kg/min) conditions. A clipped catheter was placed within the ascending aorta via the right carotid artery. The clip was released to collect two or three drops of blood. From each blood sample, 250 μl were then transferred to a test tube by use of a micropipette. Then, these samples were measured with the well counter. Sampling intervals were 5 sec during the first minute, every 10 sec for the next minute and every 20 sec for the last minute. Arterial blood was also withdrawn from the femoral artery by Harvard pump and measured with BACC-4. The dead volume from the femoral artery to the BGO detector system was ~0.9 ml. The integral values of blood sampling data were compared with those determined with BACC-4.

Statistical Analysis

Hemodynamic data were expressed as mean ± s.d. All data were analyzed by analysis of variance. If a statistical significance was obtained, we used Scheffé's criteria for multiple comparison. A two-tailed p value of <0.05 was considered statistically significant.

RESULTS

Hemodynamics

Hemodynamic data for the different pharmacologic interventions are summarized in Table 2. Compared with the control conditions, adenosine reduced systemic BP without significantly changing the heart rate. There was also a tendency for the rate–pressure product (RPP) to decrease ($p = 0.054$). Propranolol decreased the heart rate and RPP. However, there was no significant change in systemic BP. Myocardial blood flow differed significantly among the three groups. Under control and propranolol conditions, a linear relationship was observed between RPP and MBF (Fig. 1).

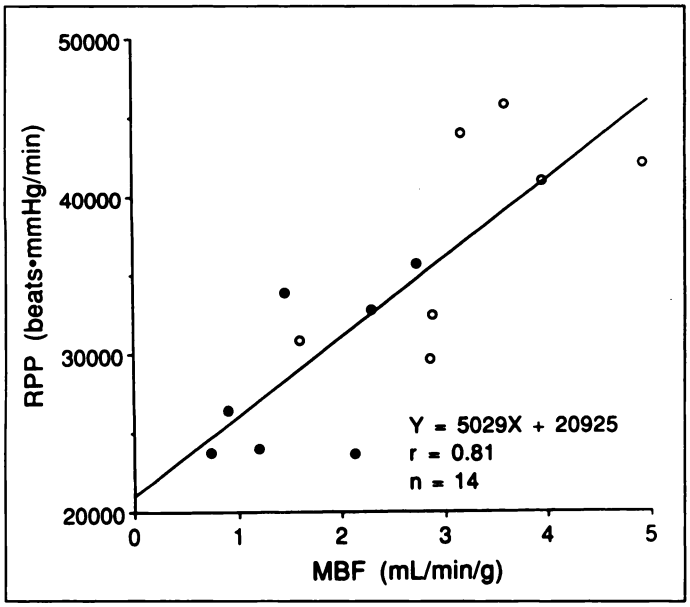

FIGURE 1. Correlation between MBF measured with microspheres and RPP. ○, control; ●, propranolol.

Arterial Input Function

Figure 2A shows the time-activity curves of the arterial input function obtained with the well counter and BACC-4. The integral values obtained from 0 to 3 min were displayed in scatterplots between the results of the well counter and BACC-4 measurements, as shown in Figure 2B. In the ^{13}N-ammonia experiments with five rabbits, with a total of 10 bolus injections under a wide range of control and pharmacologic conditions, the results yielded a correlation coefficient of 0.93.

PET Imaging

Examples of serial images are shown in Figure 3. At the midventricular level, the bolus transit through the right heart, lungs and the left heart was visualized on the second and third images. Clearance of ^{13}N activity in the blood pools and lungs occurred primarily during the first 40 sec. Thereafter, the myocardial image was delineated. Figure 4 shows a typical time-activity curve of the myocardium from the myocardial ROI in the same rabbit as in Figure 3. Figure 5 shows four contiguous midventricular summed images obtained from 3 to 6 min after the administration of ^{13}N-ammonia in a control rabbit. The myocardial image exhibited homogeneous accumulation of ^{13}N activity.

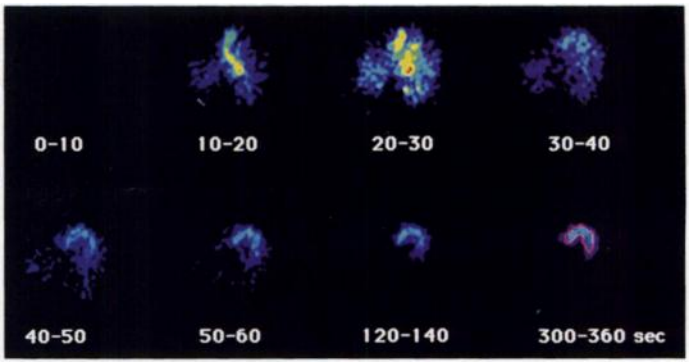

FIGURE 3. Serial PET images obtained after intravenous injection of ^{13}N-ammonia at midventricular level in a rabbit. Myocardial ROI was shown only on last image, but ROIs were also projected to early images. In these tomograms, lateral myocardium is on right, anterior is uppermost and septum is on left.

Comparison of Nitrogen-13 Myocardial Uptake with Myocardial Blood Flow Measured with Microspheres

Figure 6 shows the correlation between ^{13}N myocardial uptake obtained from PET (U) and MBF measured concomitantly with microspheres (F). Applying the Renkin–Crone model (*13,14*) to the relationship between ^{13}N myocardial uptake and MBF, we achieved the best fit for our data concerning the relationship between ^{13}N-ammonia uptake and MBF with the following equation (r = 0.88):

$$U = F \times (1 - e^{-2.7/F}).$$

The plot demonstrates that the relationship is almost linear for flows of <2.5–3.0 ml/min/g and that increases in flow lead to smaller changes in ^{13}N-ammonia uptake.

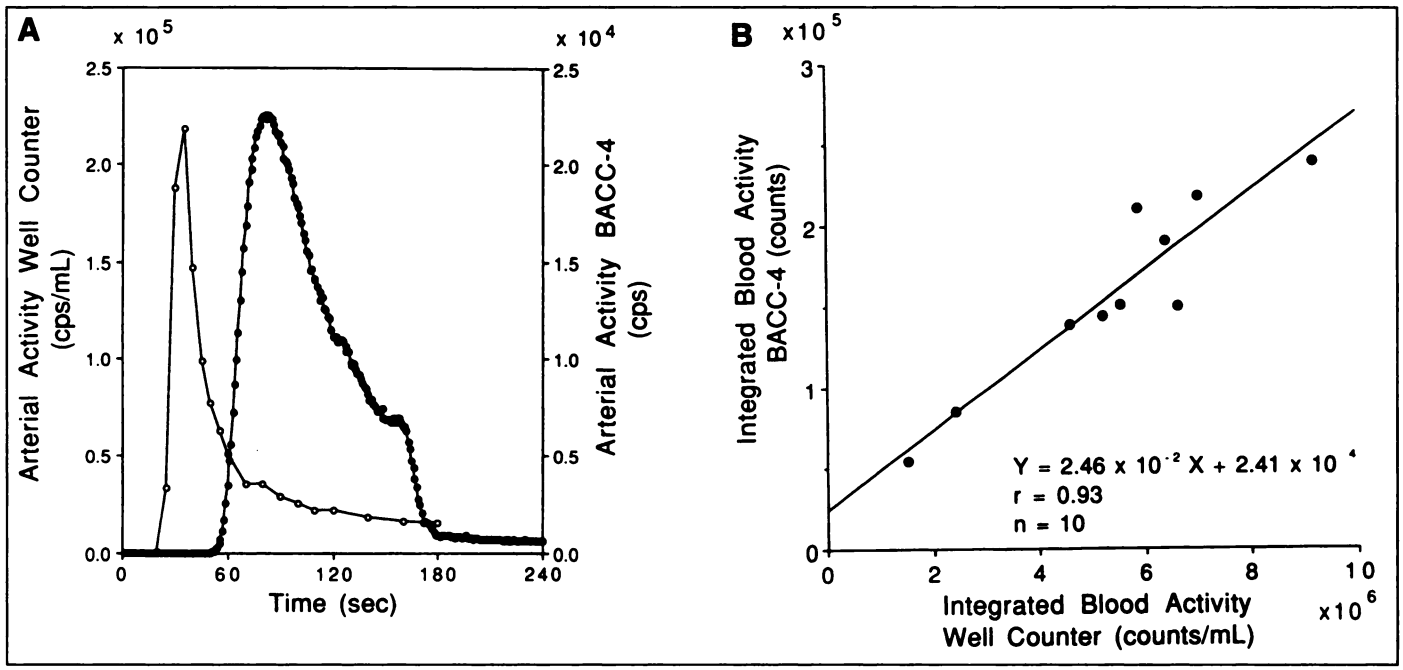

FIGURE 2. (A) Time-activity curves of arterial input function obtained by sampling directly from ascending aorta with the well counter (○) and BACC-4 (●). (B) Comparison of integral values of blood sampling data with those determined with BACC-4.

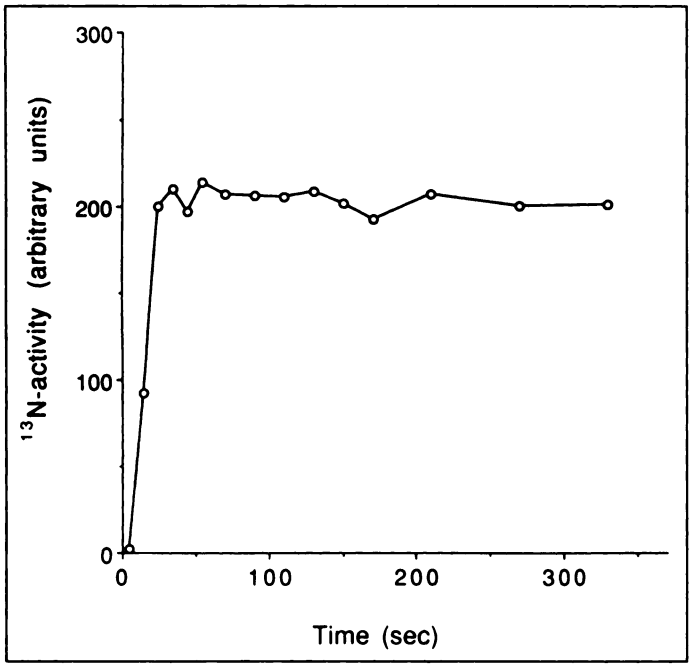

FIGURE 4. Myocardial time-activity curve in same rabbit as in Figure 3.

DISCUSSION

Quality of PET Images

The left ventricular diameter and wall thickness of a rabbit's heart are ~10–13 and 3–4 mm, respectively, with a total heart mass of ~7 g. Although the hearts were small, three or four contiguous cross-sectional myocardial images could be obtained from each after the intravenous injection of ^{13}N-ammonia. Additionally, the initial passage of the tracer through the heart was obtained with serial 10-sec PET images. The results demonstrated that dynamic physiologic processes of the tracer can be assessed even in small animal hearts. However, ECG gating of the heart may become difficult, due to the count limitation from a small heart and rapid heart rate (200–300 bpm); therefore, it was not performed in this study.

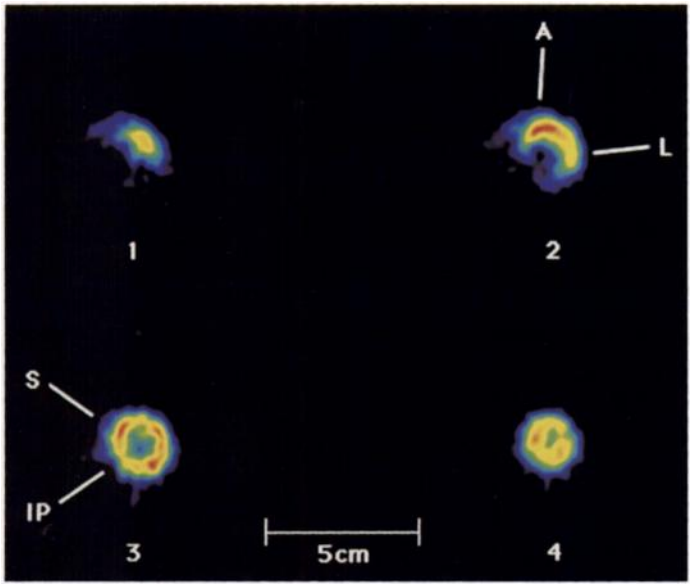

FIGURE 5. Four contiguous cross-sectional myocardial images obtained from 3 to 6 min after administration of ^{13}N-ammonia in rabbit without intervention. Uptake of tracer is homogeneous, and contrast between myocardium and both blood and lung is high. Distance between slices was 6.5 mm. A = anterior; IP = inferoposterior; L = lateral; S = interventricular septum.

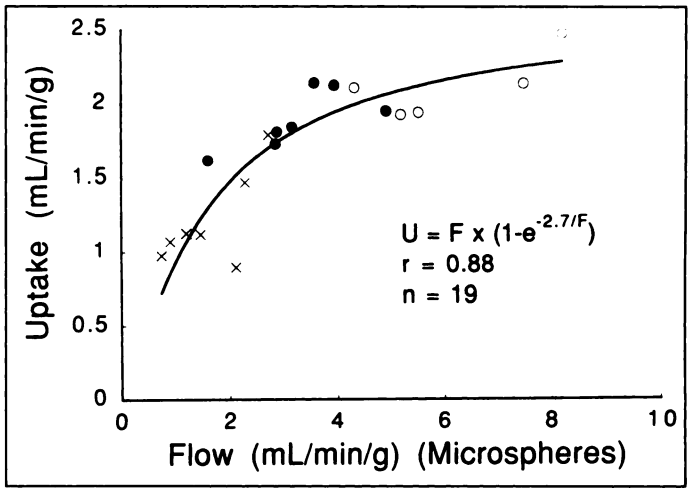

FIGURE 6. Relationship between ^{13}N myocardial uptake (extraction times flow) measured with PET and actual MBF measured with microspheres. ○, adenosine; ●, control; ×, propranolol.

Quantitation of PET Images

Spillover of activity from the blood pool to the left ventricular myocardium and partial volume effects were not corrected in this study. However, the PET activity in the myocardium was directly cross-calibrated to the well counter activity. Blood pool activity is ~6%–10% of myocardial activity at 3–4 min postinjection. The calculated spillover fraction from the blood to the myocardium is ~0.16 for a myocardial thickness of 3.0 mm and PET resolution of 3.0 mm FWHM. Therefore, the amount of spillover from the blood to the myocardium is <2% of the myocardial activity. As a result, we did not do the spillover correction for the calculation of ^{13}N myocardial uptake. If data from the early time after the tracer injection were to be used, the spillover effect from the blood to the myocardium could not be ignored. Moreover, axial resolution is coarser than transaxial resolution, which may affect the quantitation of PET images. Further studies are needed to overcome these limitations.

We used only the integral value of arterial input function for the calculation of ^{13}N myocardial uptake. There was a good correlation between the integral values of the well counter and BACC-4 measurements. Therefore, the correction of the shift and dispersion of arterial input function are not needed in this study.

Measurement of MBF

Applying the Renkin–Crone model (*13,14*) to the relationship between ^{13}N myocardial uptake and microsphere blood flow, we observe a good correlation. Although this shows that quantitative experimental studies are possible for this system, flow values greater than ~4.0 ml/min/g lead to smaller changes in ^{13}N myocardial uptake, indicating that the approach is insensitive at high flows. In rabbits, however, heart rate, arterial BP and MBF at rest are 200–300 beats/min, 90–130 (systolic) and 80–90 (diastolic) mmHg and 1.7–2.4 ml/min/g, respectively (*15*). These values are quite different from those of humans. Thus, we need to be careful when applying the results to human data. Despite species differences, rabbits are the most widely used animal model for research on cardiovascular diseases, such as atherosclerosis (*7*), because they are inexpensive, easy to maintain and handle in laboratories, large enough for sample collection, susceptible to cholesterol feeding and breed easily. Moreover, rabbits easily reproduce the pathology of human diseases, as compared to dogs and pigs. In addition, we should also take into account the issues of animal welfare,

cost and public concern. The relation of reduced coronary flow reserve and hypercholesterolemia is a current topic in the field of clinical cardiology. The ability to measure MBF in the rabbit model, in particular the hyperlipidemic rabbit, could be important in this field.

CONCLUSION

We have demonstrated the capabilities of our cardiac PET system for in vivo imaging and quantitation of MBF in small animals. This system has sufficiently high temporal and spatial resolutions to be used on small animals and may have the potential to play an important role in the study of animal models in cardiovascular diseases.

ACKNOWLEDGMENTS

We thank H. Okada, K. Shimizu and T. Kosugi (Hamamatsu Photonics K.K., Hamamatsu, Japan) for their assistance with PET imaging. We also thank Y. Kuwabara, MD (Chiba University School of Medicine), for discussions regarding statistical analysis; K. Yamada, DVM (Obihiro University of Agriculture and Veterinary Medicine) for his advice regarding our experimental setup; and Nizar A. Mullani, BSc (University of Texas Medical School at Houston), for his comments during manuscript preparation. This work was supported in part by the Japanese Special Coordination Fund for the Promotion of Science and Technology and grants from the National Cardiovascular Center, Smoking Research Foundation and Kashiwado Memorial Foundation (Japan).

REFERENCES

1. Hichwa R. Are animal scanners really necessary for PET [Editorial]? *J Nucl Med* 1994;35:1396–1397.
2. Marriott CJ, Cadorette JE, Lecomte R, Scasnar V, Rousseau J, van Lier JE. High-resolution PET imaging and quantitation of pharmaceutical biodistributions in a small animal using avalanche photodiode detectors. *J Nucl Med* 1994;35:1390–1396.
3. Westerberg G, Bergström M, Gustafson S, Lindqvist U, Sundin A, Långström B. Labelling of polysaccharides using [^{11}C]cyanogen bromide. In vivo and in vitro evaluation of ^{11}C-hyaluronan uptake kinetics. *Nucl Med Biol* 1995;22:251–256.
4. Ishiwata K, Noguchi J, Toyama H, et al. Synthesis and preliminary evaluation of [^{11}C]KF17837, a selective adenosine A_{2A} antagonist. *Appl Radiat Isot* 1996;47:507–511.
5. Elsinga PH, Vos MG, van Waarde A, et al. (S,S)- and (S,R)-1′-[^{18}F]fluorocarazolol, ligands for the visualization of pulmonary β-adrenergic receptors with PET. *Nucl Med Biol* 1996;23:159–167.
6. Osman S, Luthra SK, Brady F, et al. Studies on the metabolism of the novel antitumor agent [N-methyl-^{11}C]N-[2-(dimethylamino)ethyl]acridine-4-carboxamide in rats and humans prior to Phase I clinical trials. *Cancer Res* 1997;57:2172–2180.
7. Jayo JM, Schwenke DC, Clarkson TB. Atherosclerosis research. In: Manning PJ, Ringler DH, Newcomer CE, eds. *The biology of the laboratory rabbit*, 2nd ed. San Diego: Academic Press; 1994:367–380.
8. Yamashita T, Watanabe M, Shimizu K, Uchida H. High resolution block detectors for PET. *IEEE Trans Nucl Sci* 1990;37:589–593.
9. Watanabe M, Uchida H, Okada H, et al. A high resolution PET for animal studies. *IEEE Trans Med Imaging* 1992;11:577–580.
10. Hale SL, Alker KJ, Kloner RA. Evaluation of nonradioactive, colored microspheres for measurement of regional myocardial blood flow in dogs. *Circulation* 1988;78:428–434.
11. Yoshida K, Mullani N, Gould KL. Coronary flow and flow reserve by PET simplified for clinical applications using rubidium-82 or nitrogen-13-ammonia. *J Nucl Med* 1996;37:1701–1712.
12. Tadokoro H, Yoshida K, Takami A, et al. *A high detection efficiency BGO, flow-through, coincidence detection system for arterial blood sampling with PET: application and dispersion correction for small animal PET studies* [conference record]. 1997 IEEE Nuclear Science Symposium, Albuquerque, NM, November 1997:M10–33.
13. Renkin EM. Transport of potassium-42 from blood to tissue in isolated mammalian skeletal muscles. *Am J Physiol* 1959;197:1205–1210.
14. Crone C. The permeability of capillaries in various organs as determined by use of the "indicator diffusion" method. *Acta Physiol Scand* 1963;58:292–305.
15. Brewer NR, Cruise LJ. Physiology. In: Manning PJ, Ringler DH, Newcomer CE, eds. *The biology of the laboratory rabbit*, 2nd ed. San Diego: Academic Press; 1994:63–64.

Comparison of Four Motion Correction Techniques in SPECT Imaging of the Heart: A Cardiac Phantom Study

Michael K. O'Connor, Kalpana M. Kanal, Mark W. Gebhard and Philip J. Rossman

Department of Radiology, Mayo Clinic, Rochester, Minnesota

The aim of this study was to evaluate the accuracy of four different motion correction techniques in SPECT imaging of the heart. **Methods:** We evaluated three automated techniques: the cross-correlation (CC) method, diverging squares (DS) method and two-dimensional fit method and one manual shift technique (MS) using a cardiac phantom. The phantom was filled with organ concentrations of ^{99m}Tc closely matching those seen in patient studies. The phantom was placed on a small sliding platform connected to a computer-controlled stepping motor. Linear, random, sinusoidal and bounce motions of magnitude up to 2 cm in the axial direction were simulated. Both single- and dual-detector 90° acquisitions were acquired using a dual 90° detector system. Data were acquired over 180° with 30 or 15 frames/detector (single-/dual-head) at 30 sec/frame in a 64 × 64 matrix. **Results:** The simulated single-detector system, CC method, failed to accurately correct for any of the simulated motions. The DS technique overestimated the magnitude of phantom motion, particularly for images acquired between 45° left anterior oblique and 45° left posterior oblique. The two-dimensional and MS techniques accurately corrected for motion. The simulated dual 90° detector system, CC method, only partially tracked random or bounce cardiac motion and failed to detect sinusoidal motion. The DS technique overestimated motion in the latter half of the study. Both the two-dimensional and MS techniques provided superior tracking, although no technique was able to accurately track the rapid changes in cardiac location simulated in the random motion study. Average absolute differences between true and calculated position of the heart on single- and dual 90°-detectors were 1.7 mm and 1.5 mm for the two-dimensional and MS techniques, respectively. The corresponding values for the DS and CC techniques were 5.7 and 8.9 mm, respectively. **Conclusion:** Of the four techniques evaluated, manual correction by an experienced technologist proved to be the most accurate, although results were not significantly different from those observed with the two-dimensional method. Both techniques accurately determined cardiac location and permitted artifact-free reconstruction of the simulated cardiac studies.

Key Words: motion correction; SPECT; myocardium

J Nucl Med 1998; 39:2027–2034

Received Dec. 4, 1997; revision accepted Apr. 15, 1998.

For correspondence or reprints contact: Michael K. O'Connor, PhD, Section of Nuclear Medicine, Charlton 2N-213, Mayo Clinic, Rochester, MN 55905.